Supplementary Information

Scalable complete conversion of $MgCo_2O_4$ by mechanochemistry for high-performance supercapacitors

Zhiyuan Liu[†,‡], Qixuan Xiang[†,‡], Hao Zhang[†,‡], Xianglong Zhang[†,‡], Huijun Tan[†,‡*], Yaping Zhao[†,‡*]

[†]School of Chemistry and Chemical Engineering, Frontiers Science Center for Transformative Molecules, Shanghai Jiao Tong University, Shanghai 200240, People's Republic of China

[‡]Inner Mongolia Research Institute, Shanghai Jiao Tong University, Inner Mongolia 010052, People's Republic of China

[*]Corresponding authors: Dr. Huijun Tan, Prof. Yaping Zhao

Email: sophie93@sjtu.edu.cn (H. Tan),ypzhao@situ.edu.cn (Y.Zhao)

S1 The peaks detected in XRD and their corresponding phases

The diffraction peaks at 2θ of 19.1º, 31.4º, 37.0º, 38.7º, 44.9º, 55.8º, 59.4º, 65.3º and 77.34º correspond to the (111), (220), (311), (222), (400), (442), (511), (440), and (533) planes of standard $MgCo_2O_4$ (JCPDS No. 81-0667), respectively[1]. The peaks at 18.6º, 38.0º, 50.9º, and 58.6º correspond to the (001), (101), (102), and (110) of $Mg(OH)_2$ (ICDD No. 01-074-2220), respectively[2]. Two different MgO phases were detected. The MgO phase at 43.0º corresponds to the cubic structure with lattice constants *a* of 0.422 nm (ICDD No. 01-087-0653)[3] and another MgO peak at 48.4º corresponds to a cubic structure with lattice constants *a* of 0.384 nm (JCPDS card No 96-901-3242)[4]. The XRD peak at 2θ of 35.7 corresponds to the (311) plane of Fe_3O_4 (ICDD No. 01-075-0449)[5], which should be attributed to the contamination from the milling vessel.

Figures

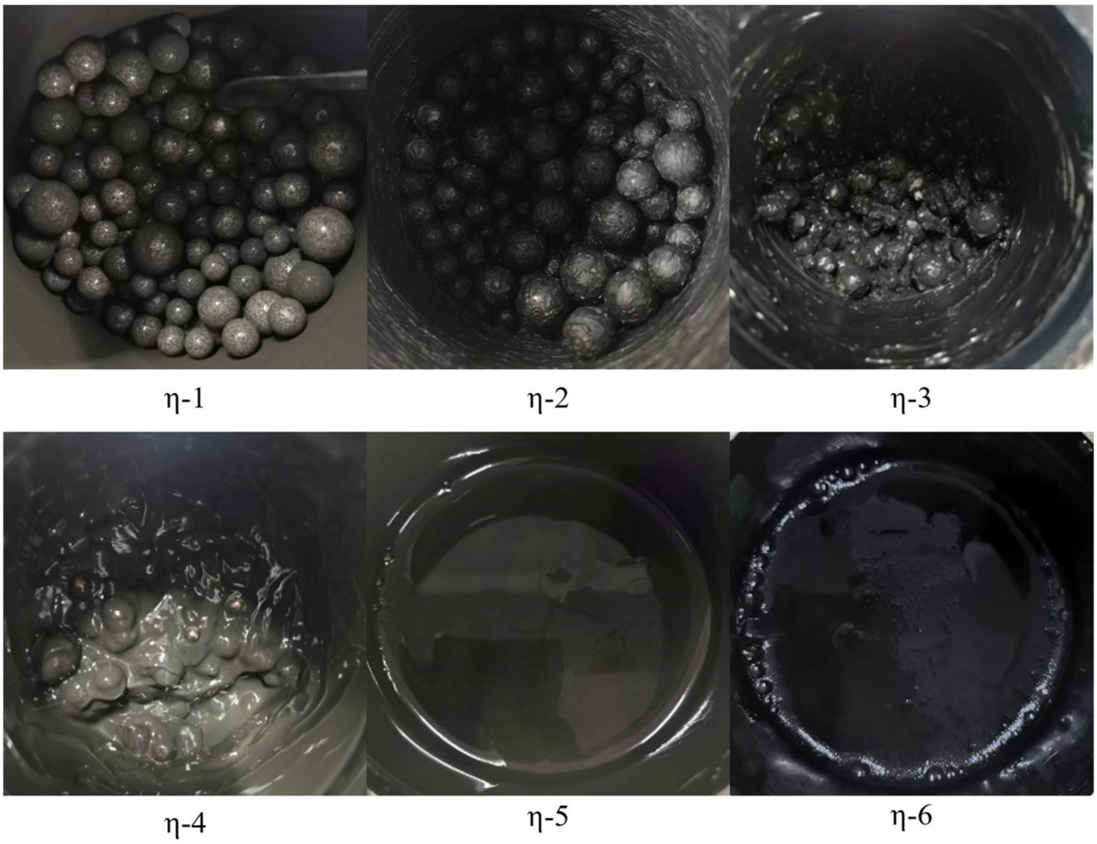

Fig. S1 The photographs of slurry in the milling vessel after ball milling for experiments in group η.

BPR-1 BPR-2 BPR-3

Fig. S2 The photographs of slurry in milling vessel after ball milling for experiments in group BPR.

Tables

Table S1 The ratio of milling balls: Diameter and wt% of grinding ZrO_2 balls used.

Ball diameter (mm)	Weight ratio (%)
15	10
12	15
10	21.5
8.5	27.1
5	13.2
3	13.2

Table S2 Measured particle size (nm) of ten individual particles in SEM images for as-prepared samples in group T.

Numbering of particle	Sample name				
	T-1	T-2	T-3	T-4	T-5
1	124.1	103.0	114.1	192.6	81.4
2	149.1	86.9	238.0	95.7	154.3
3	143.0	80.9	177.5	76.6	84.1
4	198.4	132.2	102.2	136.7	121.6
5	175.9	135.9	179.9	94.1	96.6
6	107.5	149.3	100.1	197.6	85.0
7	186.7	312.1	112.0	77.1	102.2
8	122.1	143.3	112.2	125.4	128.5
9	237.2	149.1	103.0	102.2	88.7
10	300.0	89.2	117.6	79.7	105.4
Ave. particle size	174.4	138.2	135.7	117.8	104.8

Table S3 Element analysis from EDS

Element	Atomic %	Atomic % Error	Weight %	Weight % Error	Net Counts
Mg	2.9	0.0	4.3	0.1	12 263
Co	5.9	0.1	21.2	0.4	12 648

Table S4 Measured grain size (nm) of ten individual grains in TEM image for T-4 sample.

Numbering of particle	T-4
1	19.4
2	44.9
3	18.0
4	13.7
5	12.8
6	23.7
7	10.4
8	10.6
9	23.1
10	8.6
Ave. grain size	18.5

Table S5 Coulomb efficiency calculated by galvanostatic discharge at different current densities for samples in group T.

Sample Name	Coulomb Efficiency at 0.1 A/g	Coulomb Efficiency at 0.5 A/g	Coulomb Efficiency at 1.0 A/g	Coulomb Efficiency at 2.0 A/g	Coulomb Efficiency at 5.0 A/g
T-1	92.0%	87.3%	92.1%	91.2%	91.0%
T-2	93.7%	91.2%	85.7%	85.6%	89.9%
T-3	94.6%	90.5%	92.5%	92.2%	90.3%
T-4	97.3%	93.9%	90.5%	92.6%	90.5%
T-5	90.9%	93.3%	92.7%	88.8%	80.1%

Table S6 Specific charge (C/g) calculated by galvanostatic discharge at different current densities for samples in group T.

Sample Name	Specific Charge at 0.1 A/g	Specific Charge at 0.5 A/g	Specific Charge at 1.0 A/g	Specific Charge at 2.0 A/g	Specific Charge at 5.0 A/g
T-1	144.3	102.4	95.0	82.4	65.5
T-2	240.3	187.3	140.6	115.6	88.5
T-3	247.9	190.0	171.7	151.2	121.5
T-4	266.3	235.1	194.8	175.2	138.5
T-5	155.6	138.8	125.3	106.2	76.5

Table S7 The specific charge, single batch production capacity, and the synthesis temperature of $MgCo_2O_4$ in this work and previous literature.

Morphology	Preparing Method	Specific Charge (C/g)	Single Batch Production Capacity (g)	Highest Temperature in Synthesis Process (°C)	Ref
$MgCo_2O_4$ nanofibers	Electrospun	84 at 0.5 A/g	0.1	700	[6]
$MgCo_2O_4$ spheres	Molten salt	160 at 0.5 A/g	Unknown	280	[7]
$MgCo_2O_4$ nanosheets	Hydrothermal	136 at 1 A/g	0.2	350	[8]
Porous double-urchin-like $MgCo_2O_4$	Hydrothermal	254 at 2 A/g	0.4	350	[9]
$MgCo_2O_4$ nanoflower	Hydrothermal	178 at 1 A/g	0.2	400	[10]
$MgCo_2O_4$ nanoflakes	Solvothermal	376 at 1 A/g	0.2	400	[11]
$MgCo_2O_4$ micro flowers	Solvothermal	313 at 1 A/g	0.2	350	[12]
$MgCo_2O_4$ particle	Ball milling	266 at 0.1 A/g	100	105	This work

References

1 Y. Wang, J. Sun, S. Li, Y. Zhang, C. Xu and H. Chen, Hydrothermal synthesis of flower-like $MgCo_2O_4$ porous microstructures as high-performance electrode material for asymmetric supercapacitors, *J. Alloys Compd.*, 2020, **824**, 153939–153950.

2 S. A. Walling, S. A. Bernal, L. J. Gardner, H. Kinoshita and J. L. Provis, Phase Formation and Evolution in $Mg(OH)_2$-Zeolite Cements, *Ind. Eng. Chem. Res.*, 2018, **57**, 2105–2113.

3 Q. Gu, G. Liu, H. Li, Q. Jia, F. Zhao and X. Liu, Synthesis of MgO–$MgAl_2O_4$ refractory aggregates for application in MgO–C slide plate, *Ceram. Int.*, 2019, **45**, 24768–24776.

4 M. Saket, R. Amini, P. Kardar and M. Ganjaee, The chemical treatment of the AZ31-Magnesium alloy surface by a high-performance corrosion protective praseodymium (III)-based film, *Mater. Chem. Phys.*, 2021, **260**, 124113–124125.

5 W.-W. Liu, A. Aziz, S.-P. Chai, A. Rahman Mohamed, C.-T. Tye and P. Selatan, Preparation of iron oxide nanoparticles supported on magnesium oxide for producing high-quality single-walled carbon nanotubes, *New Carbon Materials*, 2011, **26**, 225–261.

6 M. M. Ghaziani, J. Mazloom and F. E. Ghodsi, Electrospun $MgCo_2O_4$ nanofibers as an efficient electrode material for pseudocapacitor applications: Effect of calcination temperature on electrochemical performance, *Journal of Physics and Chemistry of Solids*, 2021, **152**, 109981–109991.

7 S. G. Krishnan, M. V. Reddy, M. Harilal, B. Vidyadharan, I. I. Misnon, M. H. A. Rahim, J. Ismail and R. Jose, Characterization of $MgCo_2O_4$ as an electrode for high performance supercapacitors, *Electrochim. Acta*, 2015, **161**, 312–321.

8 H. Wang, N. Mi, S. Sun, W. Zhang and S. Yao, Oxygen vacancies enhancing capacitance of $MgCo_2O_4$ for high performance asymmetric supercapacitors, *J. Alloys Compd.*, 2021, **869**, 159294–159301.

9 J. Xu, L. Wang, J. Zhang, J. Qian, J. Liu, Z. Zhang, H. Zhang and X. Liu, Fabrication of porous double-urchin-like $MgCo_2O_4$ hierarchical architectures for high-rate supercapacitors, *J. Alloys Compd.*, 2016, **688**, 933–938.

10 S. G. Krishnan, M. Harilal, I. I. Misnon, M. V. Reddy, S. Adams and R. Jose, Effect of processing parameters on the charge storage properties of $MgCo_2O_4$ electrodes, *Ceram. Int.*, 2017, **43**, 12270–12279.

11 E. Bao, X. Ren, R. Wu, X. Liu, H. Chen, Y. Li and C. Xu, Porous $MgCo_2O_4$ nanoflakes serve as electrode materials for hybrid supercapacitors with excellent performance, *J. Colloid Interface Sci.*, 2022, **625**, 925–935.

12 Y. Wang, S. Li, J. Sun, Y. Zhang, H. Chen and C. Xu, Simple solvothermal synthesis of magnesium cobaltite microflowers as a battery grade material with high electrochemical performances, *Ceram. Int.*, 2019, **45**, 14642–14651.